Analytical and Bioanalytical Chemistry
https://doi.org/10.1007/s00216-023-04760-1

CRITICAL REVIEW

Graphene-based field-effect transistors for biosensing: where is the field heading to?

Sabine Szunerits[1,2] · Teresa Rodrigues[1,2] · Rupali Bagale[1] · Henri Happy[1] · Rabah Boukherroub[1] · Wolfgang Knoll[2]

Received: 19 April 2023 / Revised: 13 May 2023 / Accepted: 16 May 2023

Abstract
Two-dimensional (2D) materials hold great promise for future applications, notably their use as biosensing channels in the field-effect transistor (FET) configuration. On the road to implementing one of the most widely used 2D materials, graphene, in FETs for biosensing, key issues such as operation conditions, sensitivity, selectivity, reportability, and economic viability have to be considered and addressed correctly. As the detection of bioreceptor-analyte binding events using a graphene-based FET (gFET) biosensor transducer is due to either graphene doping and/or electrostatic gating effects with resulting modulation of the electrical transistor characteristics, the gFET configuration as well as the surface ligands to be used have an important influence on the sensor performance. While the use of back-gating still grabs attention among the sensor community, top-gated and liquid-gated versions have started to dominate this area. The latest efforts on gFET designs for the sensing of nucleic acids, proteins and virus particles in different biofluids are presented herewith, highlighting the strategies presently engaged around gFET design and choosing the right bioreceptor for relevant biomarkers.

Keywords Graphene · Field-effect transistor · Bioreceptors · Sensing

Introduction

Field-effect transistors (FETs) are at the center of modern semiconductor technologies and are supporting a wide range of emerging applications. Despite their broad applications, voltage-driven FETs have a drawback of being highly susceptible to the overloaded gate voltage, with large voltage gate stress resulting in the breakdown of the gate dielectric or semiconductor barrier layer between the gate and the channel. The next generation of electric devices can be made a reality thanks to emerging two-dimension (2D) materials, crystalline materials with a single layer of atoms, or chemical compounds with a thickness of less than a nanometer. Carbon-based 2D materials such as graphene, as well as transition metal dichalcogenides (e.g., MoS_2, WS_2, WSe_2, $MoTe_2$), hexagonal boron nitride (h-BN), black phosphorus (BP), and transition metal oxides, have been investigated over the last decade as gate materials in FET technologies [1-4]. The first 2D material to be discovered and employed is graphene and remains the only 2D material with potential large-scale commercial applications so far. While the zero-band gap disqualifies graphene in digital circuits due to a small current on/off ratio, it has developed into a widely used gate material for biological FETs (bioFETs) and point-of-care-based biomedical devices [5]. The pioneering work of Mohanty et al. [6], using a graphene-based FET (gFET) for the detection of hybridization between single-stranded tethered DNA and its complementary sequence, generated a larger interest in integrating graphene in bioFETs. Easy operation, fast response time, real-time monitoring in a label-free manner, and access to a wider range of controlled surface chemistry approaches for anchoring bioreceptors together with multiplexing capability and possible microfluid integration are some key advantages of using graphene sensing channels in bioFETs. What makes that after all these years of scientific efforts by a large number of research laboratories and teams, the dream of a commercial gFET biosensor has not come true? The design of gFET sensors requires several key steps including the primary

Published in the topical collection *Advances in (Bio-)Analytical Chemistry: Reviews and Trends Collection 2024*.

✉ Sabine Szunerits
sabine.szunerits@univ-lille.fr

[1] Univ. Lille, CNRS, Centrale Lille, Univ. Polytechnique Hauts-de-France, UMR 8520 - IEMN, 59000 Lille, France

[2] Laboratory for Life Sciences and Technology (LiST), Faculty of Medicine and Dentistry, Danube Private University, 3500 Krems, Austria

Published online: 03 June 2023

graphene transfer to the substrate, but also a set of at least three electrodes to operate the transistor in liquid environments necessary for biological sensing. In addition, there is a need for gFET-adapted biorecognition elements allowing the specific capture of a target analyte and guiding via its affinity constant the limit of detection (LoD) of the sensor. This critical review will focus on the aspects of gFET layout and appropriate bioreceptors and their immobilization strategies, two aspects of the future of gFET biosensors.

Design considerations of biological gFETs

General consideration of biological gFETs

A typical gFET biosensor consists of a graphene channel between the source and drain electrodes on an insulating substrate. The density of charge carriers in this graphene channel, and hence the current, is modulated by a local electrostatic field, which is itself changed by modulations in the environment around the channel. The fundamental elements of a gFET are the source/drain contacts, the gate electrode, and the 2D graphene channel for sensing (Fig. 1a). Depending on the positing of the gate, one can distinguish a variety of gFET configurations including next to others back-gated, top-gated, and liquid-gated concepts. The interest in using graphene over other materials is due to its atomically thin geometry, which makes its electrical conductance highly responsive to bioreceptor-analyte binding events close to the graphene surface. The way the bioreceptor is immobilized onto the graphene channel together with its charge will influence the sensing performance of the gFET in the same manner as will be the size and the charge of the analyte. The application of a gate voltage (V_G) creates an electric field on the graphene channel, modulating the conductivity of graphene and consequently the drain-source current (I_{DS}) (Fig. 1b). In the case of gFET, such transfer curves are characterized by a minimum conductivity, the Dirac point (V_{Dirac}), which is generally observed at zero gate voltage ($V_G = 0$) (Fig. 1b). When a target molecule binds to the receptor on the graphene surface, the redistribution of electronic charge generates a change in the electric field across the FET channel region, which changes the electronic conductivity in the channel and the overall device response (Fig. 1b). While similar devices have been fabricated with silicon FETs for years, limited sensitivity and poor selectivity was achieved. Indeed, the sensitive detection of bioreceptor-analyte binding events in a gFET is related to either graphene doping effects by direct charge transfer between the formed bioreceptor-analyte duplex and the graphene channel and/or electrostatic gating effects (Fig. 1b). Gating effects are ascribed to the accumulation of charges on the graphene surface arising from bioreceptor-analyte binding, resulting in a local external voltage drop across the channel. If $V_G < V_{Dirac}$, with V_{Dirac} being the charge neutrality point equivalent to the minimum conductivity, called Dirac point, then the Fermi level is located in the valence band and holes are the majority charge carriers, conversely, if $V_G > V_{Dirac}$ then the Fermi level is located in the conduction band and electrons are the majority charge carriers (Fig. 1b). Positively charged analytes result generally in a shift of V_{Dirac} to more negative gate voltages. In contrast, the negatively charged target molecules will increase the density of holes in graphene and generate a positive shift. The left branch of the transfer curve (Fig. 1b) represents thus an increasing density of positive charge carriers (holes), while the right branch corresponds to increased negative charge carriers (electrons), both branches extending linearly from the Dirac point according to Eq. (1):

$$I_{DS} = g_m(V_G - V_{Dirac}) \text{with} g_m = (W/L)\mu C_g V_{DS} \quad (1)$$

with the slope g_m (transconductance) being depending on the width (W) and the length (L) of the graphene channel as well as on the mobility of charge carriers (μ) and the gate capacitance (C_g).

Back-gated gFETs for biological sensing

Due to the influence of the gate capacitance on I_{DS}, the choice where the gate is positioned becomes of high importance for biosensing applications. Si|SiO_2 remains the preferred substrate, owing to its well-established compatibility with nanoelectronics and the use of back-gating still seizes attention among the sensor community. Other solid substrates such as quartz [7, 8] and glass have lately been more widely used, but in connection with liquid-gated biosensing [7]. In back-gated configuration, C_g is dominated by the insulating layer separating the graphene channel from the gate which is typically 100 nm to few µm and thus requires the application of rather high V_G voltages to drive the FET device. A back-gated gFET for opioid sensing down to 10 pg mL^{-1} based on chemically bonded µ-opioid receptor proteins was recently proposed by the A. T. Charlie Johnsons's group (Fig. 2a) [9].

The gFET sensor was functionalized with a computationally designed water-soluble variant of the human µ-opioid receptor (G protein–coupled receptor) using 4-carboxybenzenediazonium tetrafluoroborate, which produced carboxylic acid sites on the graphene, which were further activated and stabilized with 1-ethyl-3-[3-dimethylaminopropyl] carbodiimide hydrochloride/sulfo-N-hydroxysuccinimide (EDC/sNHS). Electronic measurements of the source-drain current as a function of the back-gate voltage following each step of the functionalization procedure showed reproducible shifts in conductance. The proposed mechanism for the concentration-dependent change in V_{Dirac} is linked to a conformational change in the binding pocket of the µ-opioid receptor upon

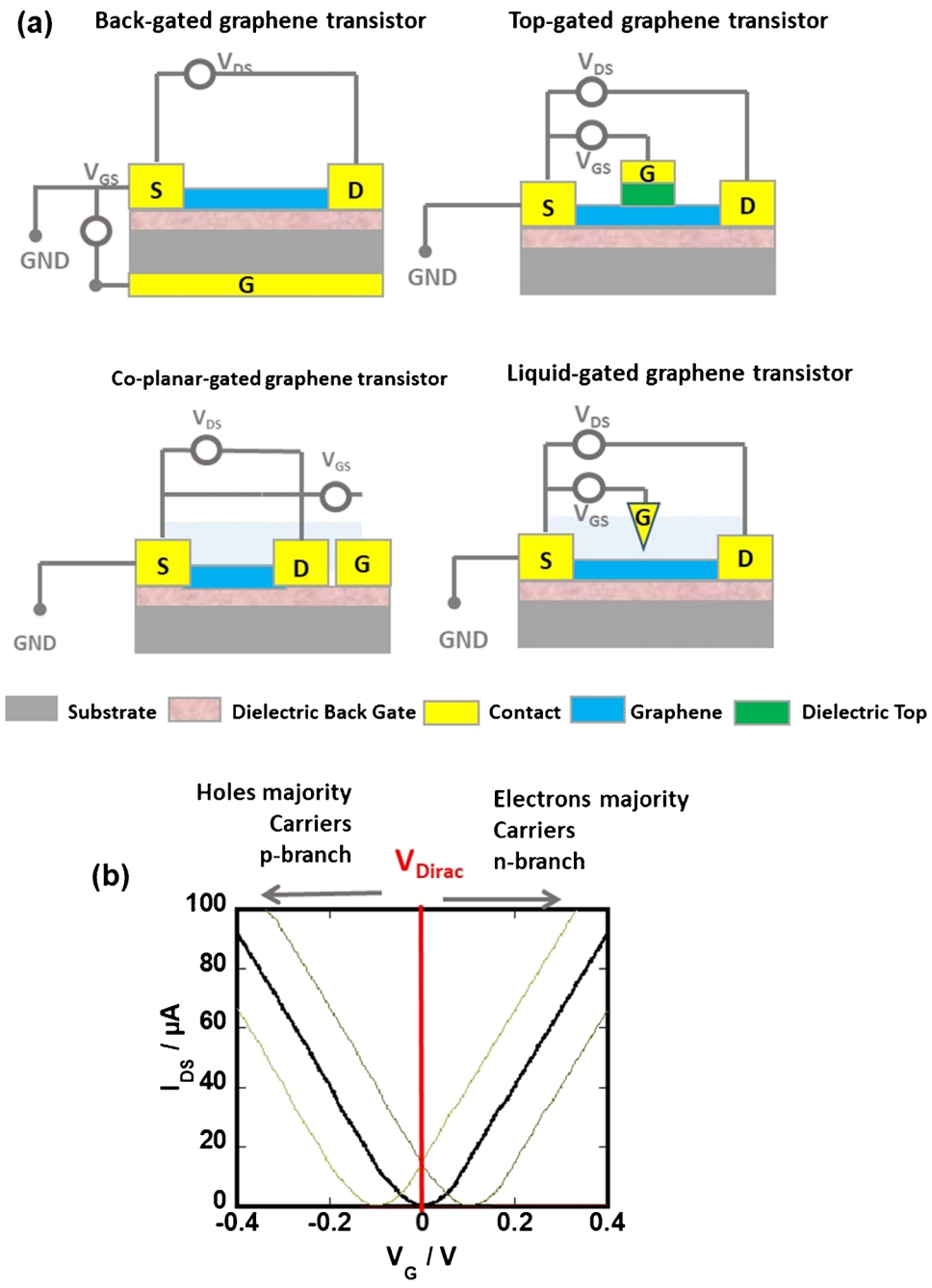

Fig. 1 Graphene field-effect transistor assemblies: **a** schematic illustration of back-gated, top-gated, liquid-gated, and co-planar configurations. **b** Transfer curves (I_{DS} *vs.* V_G) and change in position of V_{dirac} upon sensing with positively (green) and negatively (brown) charged analytes

naltrexone binding, which alters the electrostatic environment of the gFET and results in a "chemical gating effect. The possibility for the sensing of exosomes (0.1–10 µg mL^{-1}) with a back-gated antibody-modified gFET was recently demonstrated (Fig. 2b) [10]. As the exosomes are negatively charged and interact with the antibody-modified graphene channel acting as a dielectric layer, a positive charge accumulation in the graphene is detected. The maximum thickness of the functionalization layer was estimated at about 12 nm, 2 nm of the surface linkage, and 10 nm of the antibody, and sensing in low ionic strength solution (0.001×PBS) was performed only to overcome Debye length screening limitations. Interestingly binding between the exosomes and antibodies occurred under these low ionic strength conditions.

Recently, a buried-gate electrode formed via a bilayer lift-off photolithography process was proposed for interleukin-6 (IL-6) sensing [11] and overcame the requirement for the application of high V_G voltages to drive the FET device. The planar gate electrode consisting of a Cr/Au structure (2 nm/43 nm in thickness, respectively) was defined on SiO_2/Si, coated with a 30 nm HfO_2 thick dielectric using atomic layer deposition (ALD) system onto which a gold-based

drain/source electrode was formed and chemical vapor deposition (CVD) graphene transferred (Fig. 2c). The electrical signal was wirelessly transmitted to a smart-phone through a Wi-Fi connection for visualizing the trend of the cytokine concentration change reaching a LoD of 12 pM for interleukin-6 (IL-6) in saliva. This is one of the several examples of the potential of a portable gFET for disease diagnostics at an early stage in complex high ionic strength solutions such as saliva paving a new avenue for monitoring conditions of the high-risk population. Still, the construction of the device requires adapted clean room facilities making its wider application out of research laboratories currently of limited use.

Flexible electronics has become a very active research field, driven by a potentially enormous market for smart and wearable devices. Polymeric substrates such as polyimide have become attractive for flexible electronics [12-16] and flexible gFETs are an active research direction [12]. Initial steps toward developing flexible aptamer-based FET biosensors, for example, for neurotransmitter monitoring are that by Zhao et al. [14] based on nanometer-thin-film In_2O_3 back-gated FETs.

Top-gated and co-planar gated gFET-based biosensors

Top-gated gFETs are widely found in publications related to radio frequency applications [17, 18] and are indeed a suitable approach to applications where a thin oxide layer gate is advantageous to exert more control over the electrostatically doped carriers in the channel with lower gate bias required to modulate the channel. A top-gate-based electrode (10 nm/60 nm Ti/Au) (Fig. 3a) was defined for example on graphene-coated Si/SiO_2 post-modified with source and drain electrodes (10 nm Ti/50 nm Au) by a series of steps that include photolithography, e-beam evaporation, and lift-off, resulting in a top-gate channel length of 48 µm [19]. Strain sensing was performed on this device, but there is

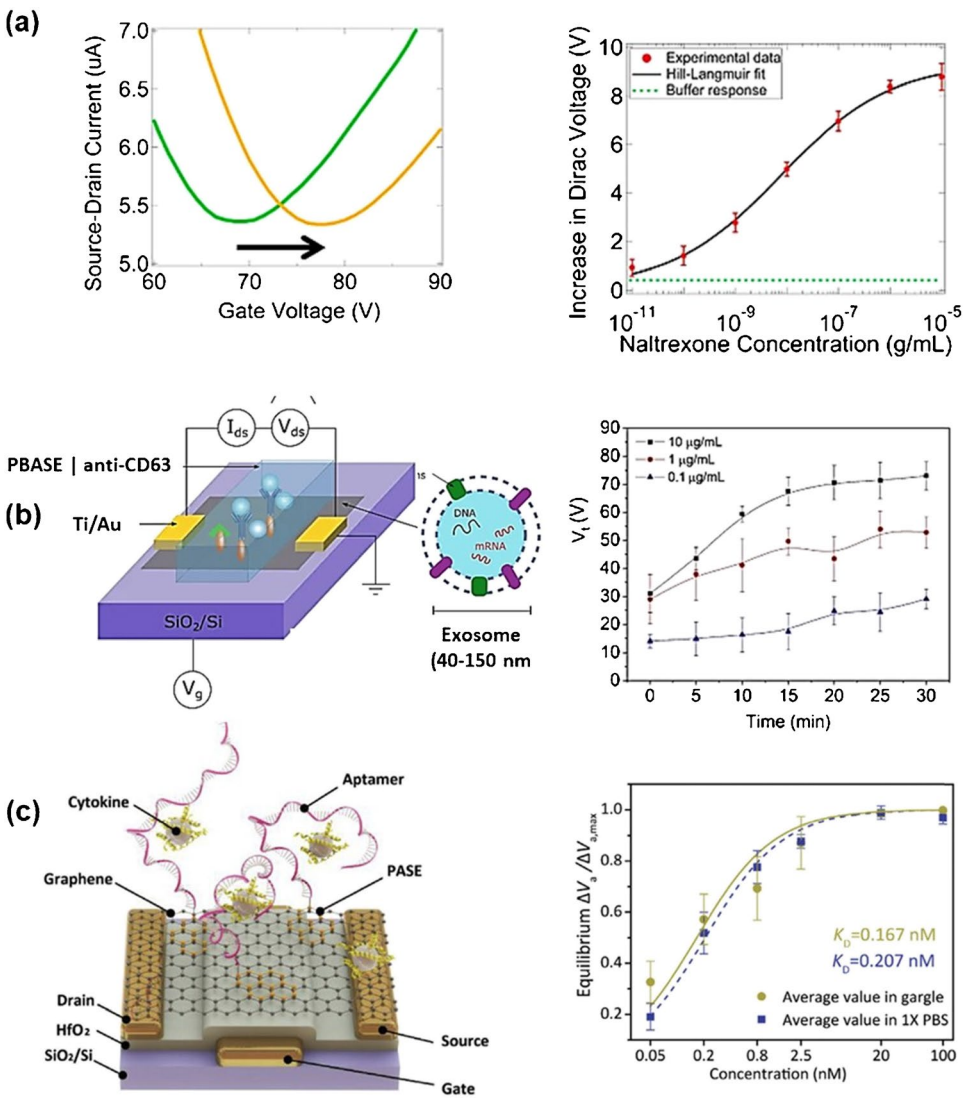

Fig. 2 Back-gated gFET for biosensing: **a** (left) transfer characteristics before and after exposure to naltrexone of a back-gated gFET array and (right) change of V_{Dirac} with increasing naltrexone concentration (reprint with permission of ref. [9]). **b** Exosome sensing on back-gated gFET modified with anti-CD63 antibody via 1-pyrenebutyric acid N-hydroxysuccinimide ester (PBASE) linkers alongside the change in V_t, being the position of the Dirac point at a given time point, over time upon addition of different concentrations of exosomes (reprint with permission from ref. [10]). **c** Buried-gate-based gFET for sensing of IL-6 by recording changes in the equilibrium $\Delta V/\Delta V_{max}$ as a function of IL-6 concentration (dashed lines are a least-squares fit to the Hill – Langmuir equation, yielding equilibrium dissociation constants (K_D) in gargle solution (green) and 1 × PBS (blue) (reprint with permission from ref. [11])

currently no biological application reported. The difficulty of growing an oxide on top of the graphene, without damaging its lattice and thus degrading the mobility of its free carriers, remains a hurdle and limits this approach strongly.

A flexible co-planar gated gFET, applied for consistent and time-resolved detection of cytokines in human biofluids and allowed for the sensitive detection of TNF-α and IFN-γ with limits of detection down to 2.75 and 2.89 pM, respectively [20]. However, this area is still in its infancy, in particular, when compared to organic field-effect transistors (OFETs) a focused research hotspot in recent years because of the fast development of flexible electronics [21].

Liquid-gated gFET-based biosensors

As biomolecules such as proteins and nucleic acids are present in biological fluids, co-planar and liquid-immersed-gate configurations are largely favored in biological gFET design as it allows for sensing in the fluid sample directly without intermediate drying steps. It is the electrical double layer (EDL) formed at the graphene/electrolyte interface rather than the position of the gate electrode which determines the capacitance as it acts like a very thin dielectric layer. The resulting capacitance (C_{total}) is much larger than that of back-gated dielectric and is determined by Eq. (2):

$$C_{total} = [1/C_q + 1/C_{dl}]^{-1} \text{ with } C_{dl} = \varepsilon_r \varepsilon_o A/\lambda_D \quad (2)$$

with C_q being the quantum capacitance originating from changes in total charge to chemical potential (Fermi level, E_F) dQ/dE_F of the 2D material, C_{dl} is the double layer capacitance of the 2D/electrolyte interface, ε_r corresponds to the relative permittivity of the electrolyte, ε_o is the vacuum permittivity, A is the area of the graphene channel, and λ_D is the Debye length. 2D materials such as graphene exhibit a high C_q and a small change in its density of state results in a significant change in its Fermi level. As C_{dl} is usually one order

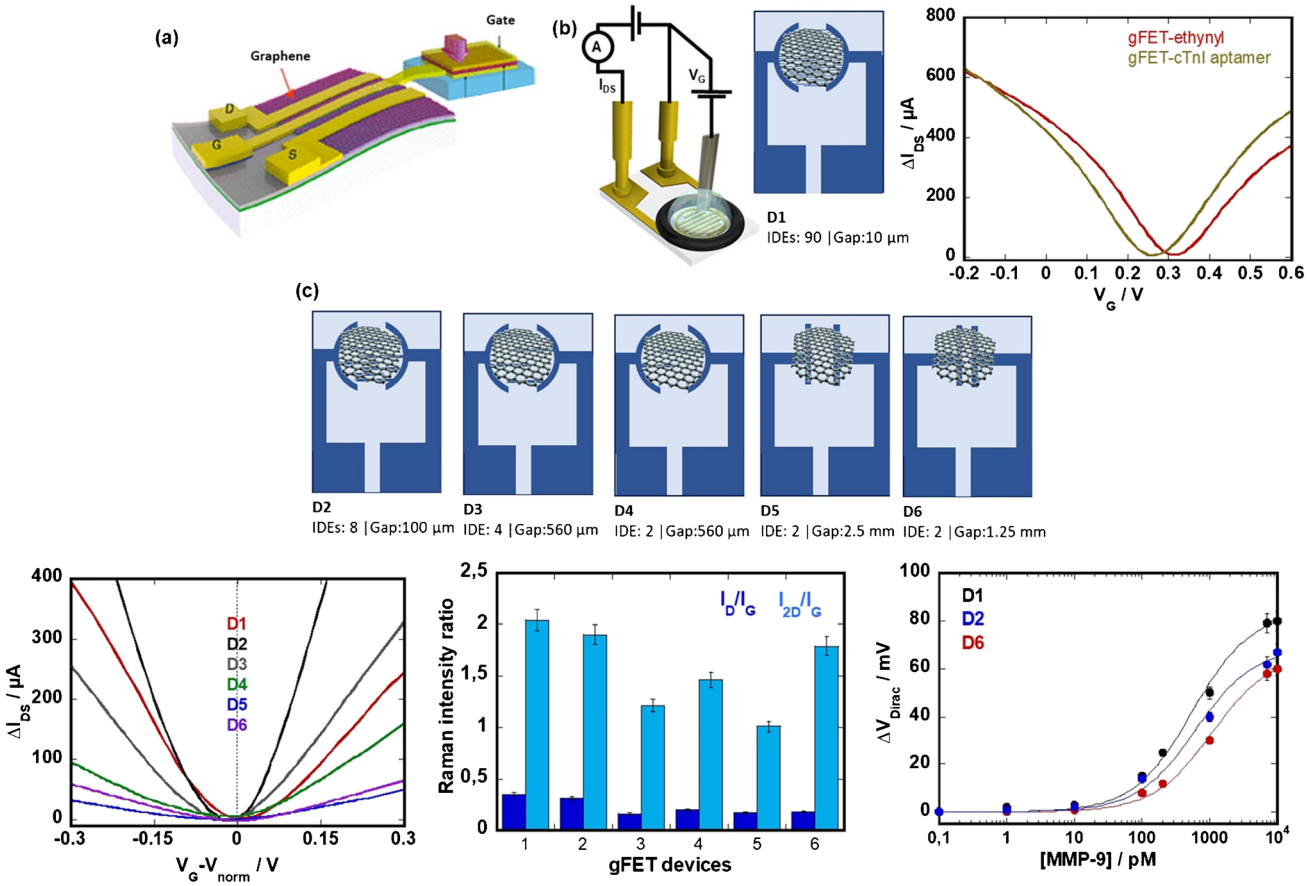

Fig. 3 Top and liquid-gated gFET for sensing: **a** top-gated gFET design coupled with biodegradable piezoelectric material–based dynamic pressure sensor (reprint with permission of ref. [19]). **b** I_{DS} *vs.* V_G of a liquid-gated gFET based on gold interdigitated electrodes (IDE) covered with CVD graphene modified with ethynyl functional groups as well as aptamers [22]. **c** Influence on IDE architecture on (left) I_{DS} *vs.* V_G curves, (middle) Ratio of I_D/I_G (dark blue) and I_{2D}/I_G (bright blue) peak intensities and (right) shift of the Dirac point upon the addition of MPP-9 in 1 × MOPS to aptamer-modified chips (unpublished results)

of magnitude larger than C_q, it leads to a dominant contribution of C_q to the total capacitance. Any accumulation of the analyte on the bioreceptors will lead to a considerable shift of the Fermi level, resulting in the high sensitivity of these gFET biosensors. This means that gate potentials applied across the EDL are at least two orders of magnitude more efficient than through the back-gate with a much smaller sweeping range of V_G required to capture the linear p and n branches being in the order of ± 1 V compared to ± 10 V for thin oxides and ± 100 V for thicker oxide layers in the back-gated configuration. The avoidance of unwanted water hydrolysis as a side reaction during the gate bias sweep in liquid media and other electrochemically driven reactions motivates the choice of the liquid or in-plane gated gFET configuration.

Our team together with others have extensively investigated interdigitated gold electrodes printed onto glass slides as a base for the construction of liquid-gated gFETs (Fig. 3b) [22-26]. Interdigitated gold electrodes (IDE) consisting of 90 electrode pairs of 10 µm in length with a 10 µm separation and a total surface area of 9.62 mm^2 (r = 1.25 mm) were coated with CVD graphene in this case. We could show that electrochemical reduction of 4 [(triisopropylsilyl)ethylenyl]benzenediazonium tetrafluoroborate (TIPS-Eth-ArN_2^+) followed by the chemical deprotection of the triisopropylsilyl (TIPS) function leads to gFET devices with largely improved drain-source current (I_{DS}) as a function of gate voltage (V_G) with hole and electron mobilities reaching 1739 ± 376 $cm^2\ V^{-1}\ s^{-1}$ and 1698 ± 536 $cm^2\ V^{-1}\ s^{-1}$, respectively [22] and well adapted for further sensing. To get a better understanding of the influence of the IDE design, the I_{DS}/V_G characteristics of gFETs formed on interfaces with a varying number of IDE (Fig. 3c) were compared. Decreasing the number of IDE further resulted in gFET with significantly lower charge mobilities in the electron and hole regions. The intensity ratio for the D, G, and *2D* Raman bands is often used as *a* criterion to assess the graphene quality. The Raman intensity ratios, I_D/I_G and I_{2D}/I_G, are comparable for all devices and indicate little defects and thus high-quality transferred graphene (Fig. 3c). Devices 1, 2, and 6 were in addition modified with an aptamer specific for MMP-9 as reported previously [27]. While devices 2 and 6 showed smaller changes in V_{Dirac}, the sensing sensitivity for MMP-9 in 1 × MOPS buffer remained comparable in all cases, suggesting no influence of the width/length ratio of the sensing channel area and charge mobility.

Gao et al. [28] reported lately the development of a flexible liquid-gated biosensor for ultra-sensitive and specific detection of miRNA with LOD as low as 10 fM within 20 min. The device was fabricated on a flexible polyimide substrate and integrated with a microfluidic chip containing an inlet and an outlet for sample loading and gate electrode placement in the liquid-gate solution. The work provides hope for developing flexible and wearable biosensor platforms for future POC diagnostics.

For liquid-gated gFETs, the Debye length λ_D (Fig. 4a), however, plays a key role in the sensing performance of the sensor. The Debye length is the distance at which the potential of a net charge is screened to 1/e of its maximum value by mobile ions in the medium. According to the Debye-Hückel model, charged molecules in solution are screened by mobile counterions such that their electrical potential is exponentially dampened with distance λ_D being the decay constant called Debye length which is given by Eq. 3:

$$\lambda_D(\mathrm{nm}) = \sqrt{\frac{\varepsilon T k_B}{2 N_A I e^2}}, I(\mathrm{mol\ L^{-1}}) = \frac{1}{2}\sum \rho_i z_i \left[\text{at room temperature } \lambda_D = 0.304/\sqrt{I}\right] \quad (3)$$

with k_B being the Boltzmann constant, T the absolute temperature, N_A the Avogadro's number, e the electron charge, I the ionic strength, and ρi and zi the density and valence of the ion species i, respectively. Charges located outside λ_D are considered out of range for electrostatic gating-based detection by a FET sensor (Fig. 4a). Under physiological conditions (> 150 mM or 1 × phosphate-buffered saline (PBS)), this accounts for λ_D = 0.7 nm, and increases to 2.4 nm (0.1 × PBS) and 7.4 nm in lower ionic strength solutions (0.01 × PBS). With the length of antibodies being around 10–15 nm or with a 30-base aptamer of about 10 nm, there is an intrinsic mismatch in dimensions between the bioreceptor and the charge screening. As pointed out lately by Soh and his group [29], the concept of double-layer crossing (orange cross section in Fig. 4a) is often overseen. Despite this challenge, the application of gFET sensors in science has been possible via the implementation of innovative strategies. To generate an electrical signal change, the target molecule's double layer (pink in Fig. 4a) must interact with the graphene double layer (yellow in Fig. 4a) (Fig. 4a). If the target creates sufficiently high double-layer potentials, signals can be detected even if the target binds many Debye lengths away from the electrode. While this concept has not been further developed until now, it was in 2015, when Gao et al. [30] demonstrated that a poly(ethylene glycol) (PEG) surface (Fig. 4b) coating decreased charge screening on FET-based biosensor and increased considerably the λ_D. It was shown that the detection of prostate-specific antigen (PSA) in 0.1 M PBS buffers is possible by co-immobilizing a PSA-specific aptamer on the electrode alongside the PEG coating (Fig. 4b) [30]. Indeed, next to the well-organized charged layer on top of graphene and guiding the Debye length, in the presence of a PEG layer on graphene, any charges or dipoles leading to a charge within that immobilized ion-permeable layer requires an extra accumulation of

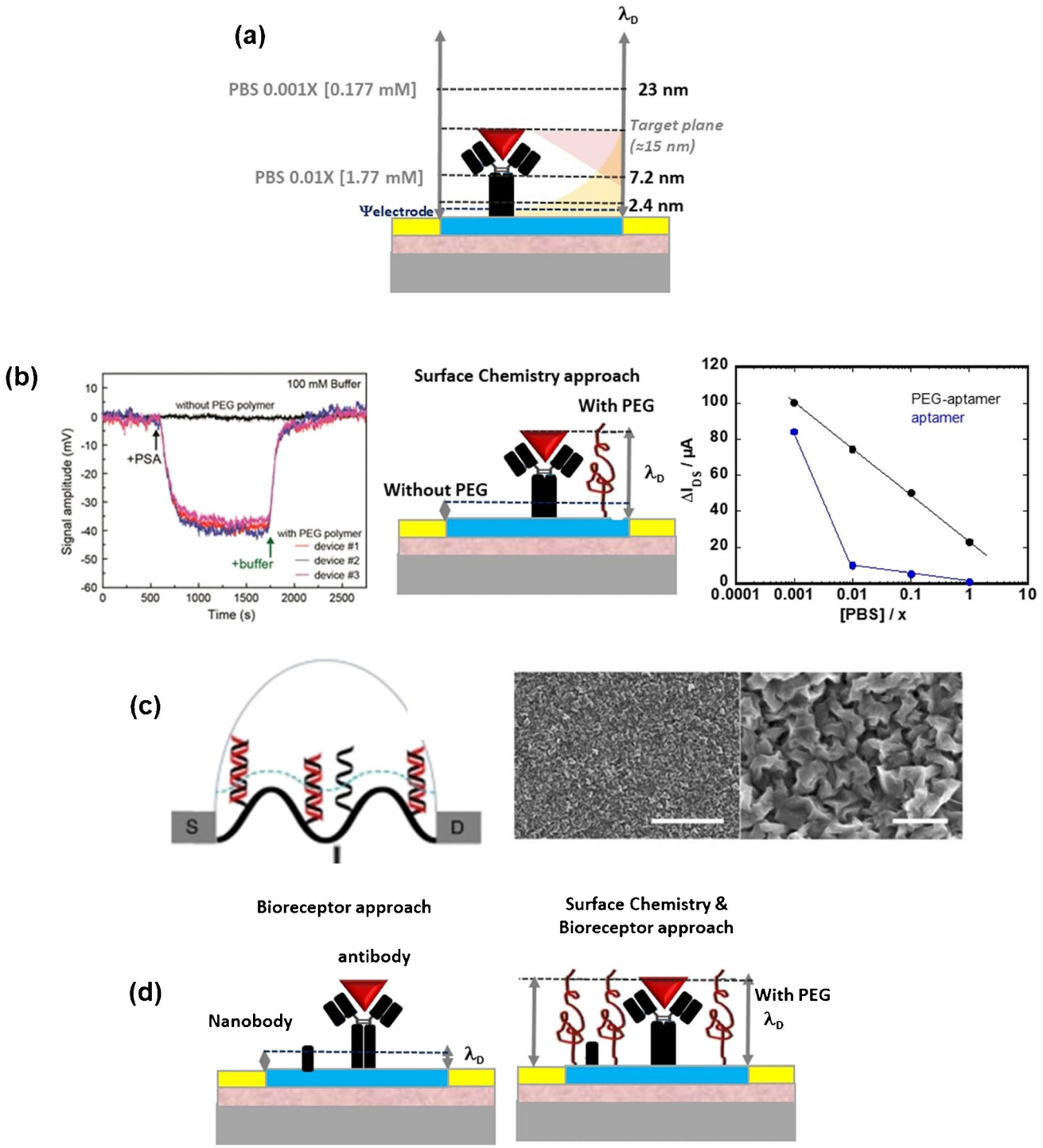

Fig. 4 Debye length screening hurdle and different strategies to overcome this for gFET biosensors: **a** correlation of bioreceptor size with Debye screening length in solution of different ionic strengths. The electrical double layer formed on the graphene interface is in yellow and that of the analyte is shown in pink. The cross section of these electrical double layers is in orange. **b** Effect of high molecular mass poly(ethylene glycol) (PEG)-modified gFET on the Debye length and its effect on the concentration-dependent measurements of PSA (10 nM) in 100 mM PB (reprint with permission from ref. [30]) as well as the obtained change of I_{DS} *vs.* the PBS concentration of the aptamer only, and for the aptamer/PEG gFET [23]. **c** Scheme of crumpled gFET DNA sensor where the blue dot lines represent the Debye length in the ionic solution. SEM images of crumpled graphene: scale bar is 5 μm (left) and 500 nm (right) (reprint with permission of ref. [37]). **d** (left) Use of nanobodies instead of antibodies and (right) a combined strategy of nanobodies and PEG chains to overcome Debye limitations

a counter-ion within the layer to maintain charge neutrality. This difference in the concentration of ions between the bulk solution and that in the immobilized protein layer creates a Donnan potential extending beyond the Debye length, in this ion-permeable PEG [31, 32]. The partially hydrated PEG changes the interfacial capacitance of the gFET with higher molecular weight PEG being preferable over lower weight ones. Too long PEG chains will however increase binding kinetics due to diffusion limitations between the bioreceptor and the analyte via the PEG layer [33]. Since then, PEG has become essential in gFET sensing for overcoming fouling issues as well as Debye length screening effects.

We together with others have followed a similar approach for the sensing of cardio troponin I (cTnI) in serum of patients [23] using a liquid-gated gFET configuration. The device responses were, as excepted, sensitive to the ionic strength of the solution as seen upon the change in I_{DS} of the aptamer:PEG-modified GFETs upon exposure to 240 pg mL^{-1} of cTnI in PBS at different concentrations (Fig. 4b). The change in I_{DS} was smaller upon increasing ionic strength solution with signals detectable in 0.1 M clearly, while an aptamer-only-modified gFET revealed no current change already in 0.01 M PBS. To push further and realize sensing in serum samples, de-salination of the serum through a Sephadex® (cross-linked dextran gel) G-25 column using gravity for separation allowed to identify correctly cTnI concentration in 15 patient samples grouped according to the magnitude of perioperative myocardial injury risk for a myocardial infraction as mild (cTnI < 15 pg mL^{-1}), moderate (15 pg mL^{-1} > cTnI < 500 mL^{-1}), and severe (cTnI > 500 pg mL^{-1}) [34]. In addition, the PEG unit worked as an antifouling matrix. As-deposited graphene is commonly hydrophobic and promotes adsorption of species possessing hydrophobic components such as proteins. These hydrophobic interactions are entropically favorable in an aqueous electrolyte, because water molecules are released from the solvation shell around hydrophobic analytes and are typically irreversible in an aqueous electrolyte under mild conditions. Therefore, many antifouling strategies aim at reducing fouling by increasing the hydrophilicity of the electrode surface and thus limiting or even preventing direct contact of antifouling compounds with the electrode-anchored bioreceptors to minimize false positive responses [35, 36].

Another concept was lately put forward by Hwang et al. [37] using a deformed monolayer graphene channel (Fig. 4c). Computational simulations revealed that the nanoscale deformations could form "electrical hot spots" in the sensing channel which reduce the charge screening at the concave regions. The increased Debye length at the convex region of the crumpled graphene brings more DNA strands inside the Debye length, making crumpled graphene electrically more susceptible to the negative charge of DNA and the change upon hybridization. This device achieved an ultra-high sensitivity of detection in buffer and human serum samples down to 600 zM and 20 aM, respectively, which correspond to ~18 and ~600 nucleic acid molecules. Moreover, the deformed graphene could exhibit a band gap, allowing an exponential change in the source-drain current from small numbers of charges.

Besides these materials and surface chemistry–based consideration, replacing a typical antibody probe of 10 nm with smaller bioreceptors, such as aptamers and nanobodies, is another way to limit signal screening issues (Fig. 4d).

Aptamers, artificial single-stranded oligonucleotides, typically 15–70 bases in length, and generally designed by Systemic Evolution of Ligands by Exponential Enrichment (SELEX), are well adapted for gFET biosensing due to their good thermal stability, low-cost (once the sequence has been identified by SELEX), and tuneable affinity to the analyte [38, 39]. With a probe length of < 5 nm for aptamer sequences of less than 30 bases, they are well adapted for gFET sensing even in higher salt solutions [40] (Fig. 4d). One of the first aptamer-modified gFET sensors is that reported by Ohno et al. [41] using an immunoglobulin E (IgE) aptamers with an approximate height of 3 nm and a K_D = 47 nM. Kim et al. [42] showed that replacing a typical antibody receptor of 10 nm with a 4 nm aptamer probe, on otherwise similar gFET sensors, improved the sensitivity to the target antigen by 1000 times from 12 fM to 10 aM in 10 µM PBS (λ_D = 23.6 nm). The signal was, however, completely screened in 1 mM PBS (λ_D = 2.3 nm) even with the small aptamer probes [42]. The possibility to tune the aptamer density on gFET sensors was assessed by Hao et al. [40] by using a novel immobilization method based on the application of an electrical field (Fig. 5a). Using 1-pyrenebutanoic acid succinimidyl ester (PBASE) as a linker representative, application of an electrical field arranged the electron-rich pyrenyl group toward graphene, resulting in regularly aligned PBASE in the solution due to electrostatic repulsion. The LOD for interleukin-6 (IL-6) could be significantly improved to 618 fM, by applying an electric field at − 0.3 V for 3 h during PBASE immobilization [40].

We have lately validated that aptamer/PEG-based gFET architectures allow for the detection of metalloproteinases such as MMPs-9, zinc-dependent endoproteinases upregulated in non-healing wounds from 1.5 to 912 pM (0.1–60.8 ng mL^{-1}). A LOD of 478 pM was determined in simulated wound fluids from the change in drain-source current at a V_{Gate} = 0 V [27] (Fig. 5b).

While DNA-based aptamers are widely employed as bioreceptors in gFET, the use of peptide nucleic acids (PNAs) has proven challenging, due to the absence of selection methods for the discovery of suitable bioreceptors and the difficult mimicry of established DNA-based ones. Despite the fact that PNAs exceed homologous DNA or RNA in terms of complementary base pairing, they can fail to

reproduce alternative modes of binding, because of their different structural features. The remarkable stability and charge distribution of PNAs were lately proven to be beneficial for gFET-based sensing of cTnI (Fig. 5c) [26]. While the affinity of the DNA aptamer toward cTnI depends both on the ionic strength and pH of the medium, with K_D increasing upon enhancing ionic strength and pH (Fig. 5c), the PNA aptamer recorded unchanged K_D values under all experimental conditions. Though the PNA aptamer has not a dramatically higher affinity for cTnI and no better detection limit, 6.0 ± 1.0 pg mL^{-1} (PNA aptamer) and 3.3 ± 0.7 pg mL^{-1} (DNA aptamer), it does help in reducing the influence of pH and ionic strength parameters, showing more stable and consistent K_D values, thus allowing for more adaptability to different conditions in the sample matrices. One main advantage of the use of a PNA aptamer in sensing is the lack of enzymatic degradation.

Next to aptamers, antibody fragments and engineered antibodies are ideal for gFET-based sensing [43] (Fig. 6a)

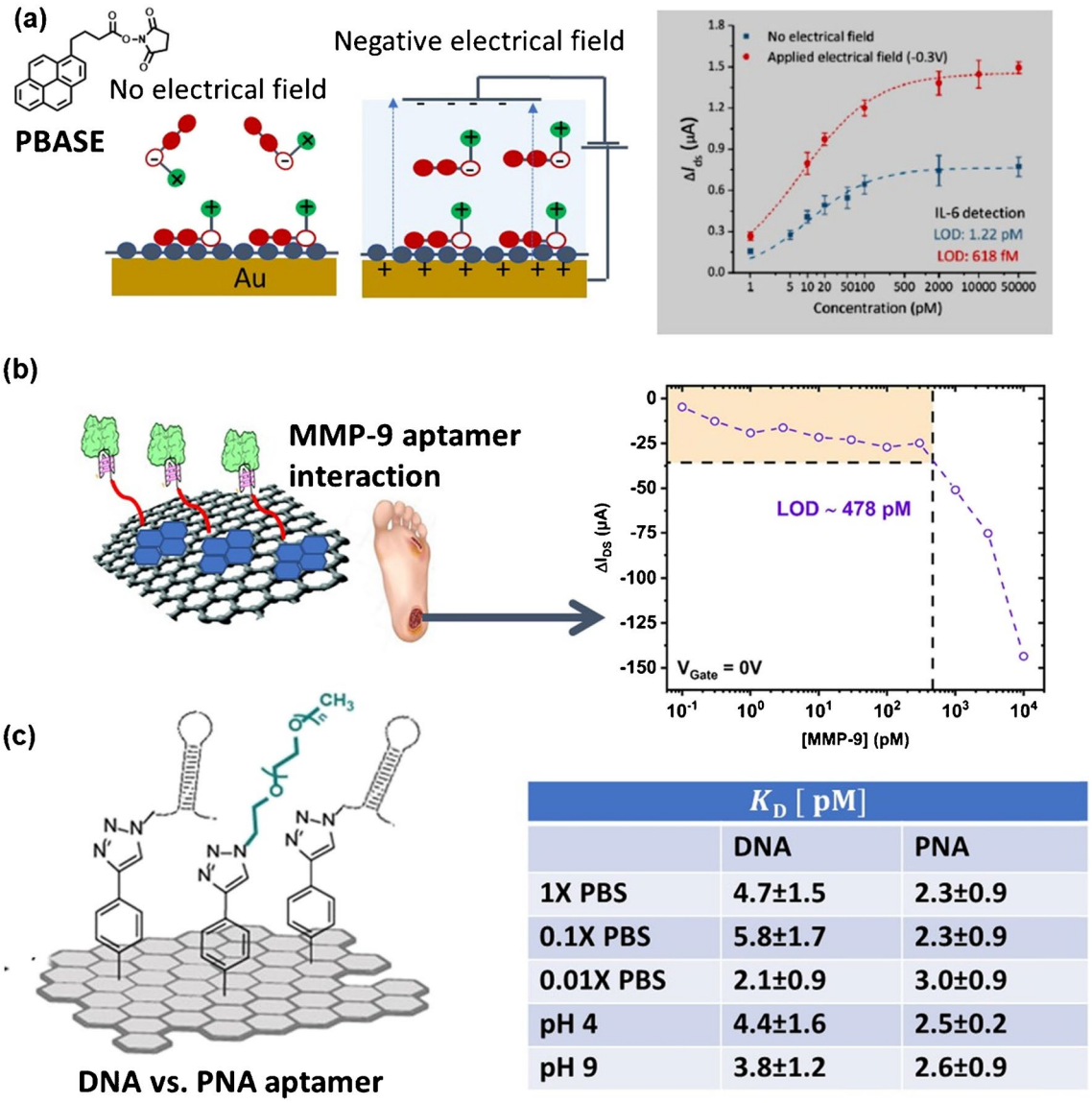

K_D [pM]		
	DNA	PNA
1X PBS	4.7±1.5	2.3±0.9
0.1X PBS	5.8±1.7	2.3±0.9
0.01X PBS	2.1±0.9	3.0±0.9
pH 4	4.4±1.6	2.5±0.2
pH 9	3.8±1.2	2.6±0.9

Fig. 5 Aptamer-based gFETs: **a** IL-6 detection in 1 × PBS with and without applied electrical field during PBASE immobilization. Without an applied electrical field, PBASE is randomly immobilized on the gFET surface, while a negative potential arranges PBASE regularly with pyrene groups forced toward graphene (reprint with permission of ref. [40]). **b** Matrix metalloproteinase-9 (MMP-9) sensing in swab samples from patients with diabetic foot ulcers on an aptamer-modified liquid-gated gFET device recording a LOD of 478 pM in MMP-9 spiked wound fluid composed of 5.8 g NaCl, 3.3 g $NaHCO_3$, 0.2 g KCl, 0.2 g $CaCl_2$, 33.0 g BSA in 1L 1 × MOPS buffer/1 mM $CaCl_2$ [27]. **c** Anchoring of cTnI-specific DNA or PNA aptamers on PEG-modified graphene and electrically determined dissociation constants against cTnI target [26]

as their performance has already been established in electrochemical sensors [44].

Indeed, antigen-binding fragments (Fab) are capable of recognizing a target molecule with high binding affinity and specificity. As the vertical length of a Fab is approximately 6 nm, these receptors can recognize and bind target antigens near the gFET surface. The probably smallest receptor units currently at hand are nanobodies, corresponding to antibodies devoid of a light chain and lacking the CH1 domain. They possess several key features such as small size (i.e., 4 nm in length, 2.5 nm in width, and about 15 kDa in molecular weight), high solubility, high chemical stability, and improved shelf-life, making them attractive for gFET-based sensing. These single-domain binding proteins are produced cheaply in microbial hosts, have better engineering profiles, and have the potential to reduce the high cost associated with monoclonal antibodies [45-47]. The

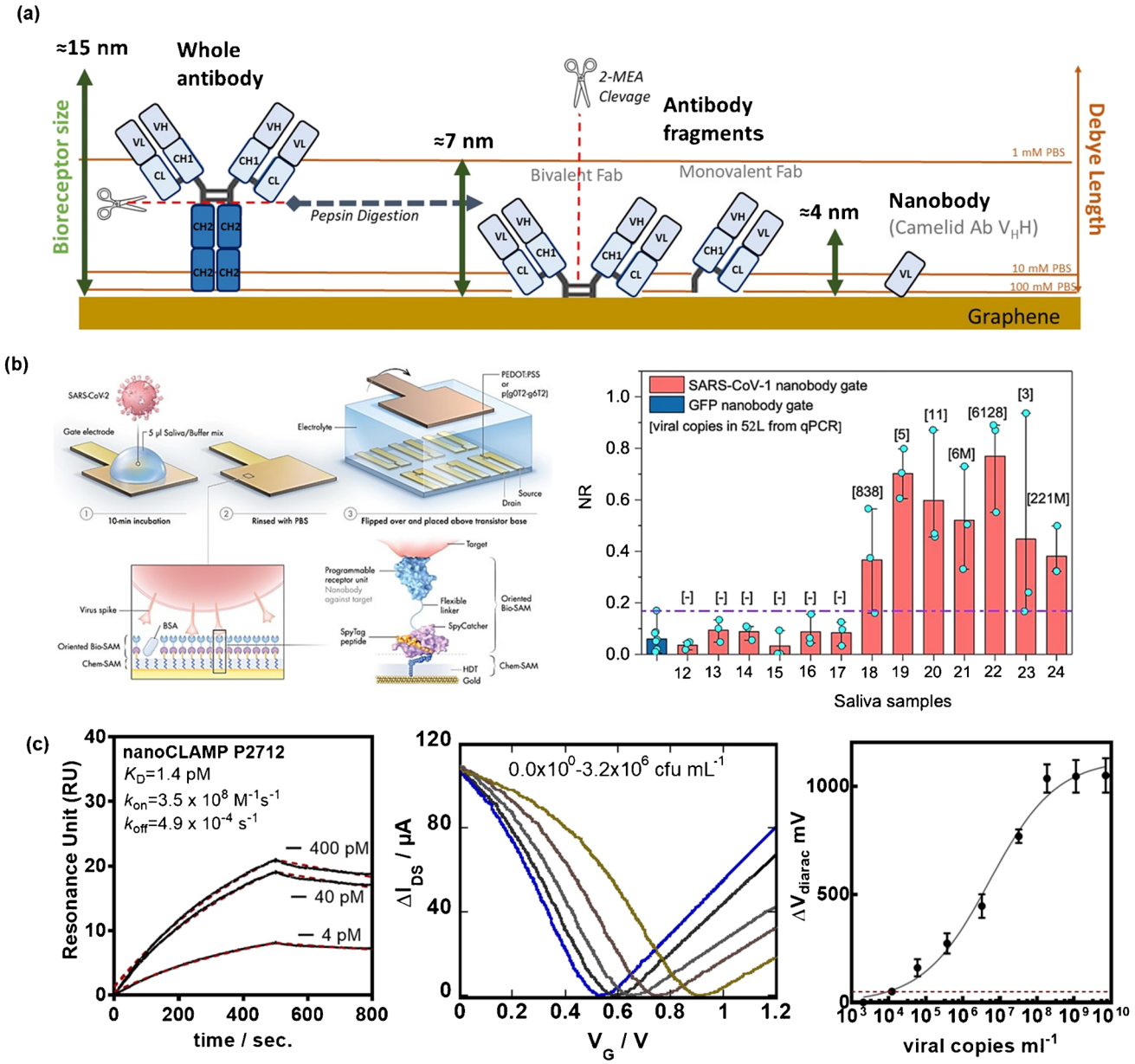

Fig. 6 From antibody fragments to nanobodies for gFET sensor: **a** correlation of antibody and antibody fragments length with Debye length in solutions of different ionic strength. **b** Schematic of a nanobody-functionalized organic electrochemical transistor sensor with a nanobody–SpyCatcher fusion protein attached to gate as bioreceptor together with sensor response for saliva sample from COVID-19-positive samples (reprint with permission from ref. [45]). **c** SPR affinity studies of nanoCLAMP P2712 specific to SARS-CoV-2 S1 protein and transfer curves of a liquid-gated gFET modified with nanoCLAMP P2712 and titrated against increasing concentrations of patient-derived viral particles (unpublished results)

reduced size of these receptors enables a binding reaction to occur more closely to the sensor surface, i.e., within the Debye length. The effect of probe molecule size on the detection of a tumor marker, α-fetoprotein (AFP), using a FET biosensor was shown by Cheng's group [48]. The team of Inhal [45] used the concept of a flexible spyTag-SpyCatcher nanobody architecture on 1,6-hexanedithiol-modified gold gates for the sensing of COVID-19 and MERS antigens in nasopharyngeal as well as in saliva samples (Fig. 6b).

While nanobodies dominate this field, their development typically originates in immunized Camelidae, followed by cloning and development of the binding domain (the nanobody), adding time to their production. Furthermore, many camelid-derived nanobodies contain disulfide bonds, making them susceptible to reducing environments, forcing them to be produced in the periplasm of *E. coli*, or in secretion expression systems, and precluding their engineering with sulfhydryl reactive probes and reagents. A different class of antibody mimetics called nanoCLAMPs (nano-CLostridial Antibody Mimetic Proteins) [49] can be screened from a synthetic, naïve phage display library of 1×10^{10} variants for high specificity, and low affinity to targets in 6 weeks; they are produced and purified cheaply from the cytosol of *E. coli* with yields above 200 g L^{-1}. They are naturally devoid of cysteine groups, and easily refolding following chemical denaturation with 6 M GuHCl, 0.1 N NaOH, or DMF when conjugated to solid support. They exhibit high thermal stability ($T_m > 65$ °C). We have lately investigated this concept using nanoCLAMP P2712 [50], showing picroMolar affinity for the S1 spike protein of SARS-CoV-2 (Fig. 6c). Viral titration experiments in liquid-gated gFETs modified with nanoCLAMP 2712 revealed that the gate voltage shifts upon increasing viral copies with a LOD of about 1.2×10^4 viral copies mL^{-1}.

Conclusion and perspectives

While 10 years ago, some of us focused on advances in graphene-based plasmonic surfaces and the interest in analytical chemistry (Anal. Bioanal. Chem. 2013, 405, 1435), in this critical review, we present some of the progress achieved in the last years on the fabrication of gFET devices to detect a large range of biomarkers (Table 1). But what makes gFET superior to other semiconductor transistor sensors? The use of a 2D channel material has indeed several advantages over bulk semiconductor devices. For most semiconductor transistor sensors (including silicon), electric field changes at the channel surface have limited effect deeper in the device channel, limiting the response sensitivity. In the case of a gFET, the graphene channel has a sub-nanometric thickness making that any analyte binding to the surface of the graphene channel impacts electronic transfer through the entire depth of the device. Other bulk semiconductors are not effective at such a thickness, as surface defects dominate the material characteristics. Furthermore, graphene is chemically stable; it is composed of very short, strong, covalent bonds, all in the plane of the film. The conductivity, stability, uniformity, and 2D nature of graphene make it an excellent material for sensors, overcoming the failings of silicon chemical and biological sensors. As non-specific protein-based bioreceptor

Table 1 Summary of gFET sensors discussed in this review

gFET type	Analyte	Bioreceptor	LoD	Comments	Ref
Back-gated	Opioid	μ-opioid protein	10 pg mL^{-1}	V_{Dirac} as high as 70–80 V	[9]
Back-gated	Exosomes	Antibody	0.1 μg mL^{-1}	Validation in low ionic strength conditions (0.001 × PBS)	[10]
Buried-gate	IL-6	Aptamer	12 pM	Saliva-based sensing	[11]
Co-planar flexible	TNF-α IFN-γ	Aptamer	TNF-α 2.75 pM IFN-γ 2.89 pM	Artificial tears	[20]
Liquid-gated flexible	miRNA	DNA	10 fM	Wearable approach	[28]
Liquid-gated	MMP-9	Aptamer	478 pM	Sensing in wound fluid	[27]
Liquid-gated	cTnI	Aptamer	3.3 pg mL^{-1} (DNA aptamer) 6.0 pg mL^{-1} (PNA aptamer)	Sensing in serum	[23, 26]
Liquid-gated	DNA	DNA	20 aM (serum) 600 zM (buffer)	Deformed monolayer graphene	[37]
Liquid-gated	Immune-globulin E	Aptamer	10 aM	Validated in 10 μM PBS, in 1 mM PBS no signal	[41, 42]
Liquid-gated	IL-6	Aptamer	618 fM	Electrical field arranged	[40]
Liquid-gated	SARS-CoV-2	NanoCLAMP	1.2×10^4 viral copies mL^{-1}	Nasopharyngeal samples	Unpubl

binding is undesirable as it often implies loss of the protein's functional structure, appropriate attachment chemistries are required. Being composed of carbon, a large range of surface chemistries are available for correct bioreceptor integration and enabling highly sensitive, highly selective, direct, label-free detection of targeted analytes.

Despite the significant progress made in aligning gFET biosensors with life sciences and their integration into microelectronic platforms, various obstacles remain to be overcome. While 2D materials provide a route to achieve device-to-device consistency, the graphene science and technology roadmap published by the Graphene Flagship indicated the target of gFET biosensors to be reached in 2022, with bioelectronic medicine, drug delivery being the focus next to neural interfaces and flexible devices from 2023 to 2030 (https://graphene-flagship.eu/innovation/industrialisation/roadmap/). Although gFET sensors have fabrication advantages over devices fabricated with 1D materials (e.g., carbon nanotubes, nanowires) as graphene can be produced in films with uniform material characteristics, the promises of gFET biosensors have not been demonstrated until now. Questions about the device structure, batch-to-batch heterogeneity, bioreceptor anchoring approaches, and consideration of how to increase Debye length are some of the difficulties that still need to be addressed for gFET commercialization. The production of gFETs with low device-to-device variation is an industrial challenge, with various European actors (e.g., Graphenea-Spain, Grapheal-France, Applied Nanolayers-Netherlands, Paragraf-Uk) working actively to overcome this hurdle. In work coming out of research laboratories, inter-device variability is mostly inconsistently assesses as a limited number of devices is investigated. The characterization of gFET ensembles of 15–30 active devices and 15–30 controls would allow a statistically robust analysis of gFET performance, essential toward clinical application. Indeed, the use of proper positive and negative controls as widely used in lateral flow assays for example is often missing in addition but essential to validate that the sensor is functioning as expected; graphene functionalization aspects should be jointly considered by academic and industrial partners including end-users to drive this field faster to an end product, a biological gFET. While, the use of gFET sensors for the detection of proteins (e.g., cTnI) as well as small molecules such as naltrexone at pgmL-1 concentrations could be shown, to improve the sensitive sensing of a large variety of analytes, the implementation of engineered single-chain variable fragments and nanobodies instead of full antibodies as receptor molecules should be more widely considered. The improved sensitivity of gFET sensors functionalized with these engineered antibodies is attributed to the closer proximity of the bound biomarker target to the gFET channel, thus leading to stronger electrostatic interactions and a larger electrical signal.

In parallel to considering "smaller" bioreceptors, efforts to create stable, density-controlled, protein antifouling functionalization strategies on graphene including ionic membrane to overcome Debye length screening limitations and to sense under physiological relevant conditions remain limited investigated. The use of multi-step surface chemistry approaches remains furthermore a hurdle for the wider implementation into most industrial processes. Innovations for single-step graphene modifications and advancements in this direction would be a breakthrough and open the way for the first European gFET-based sensor product on the market. It would also be a foundation for the next generation of health monitoring via point-of-care testing concepts to put the patient into the center of action. Portable and wearable devices gFET sensors provide a simple and veritable way in this direction. Innovation around the improvement of graphene inks for the development of flexible low-cost biosensors for high-speed printing is required to drive this field further. These wearable devices require input and power systems to command information and supply energy, respectively, and the road map of gFET sensors is strongly intertwined with these activities.

Funding Financial support from the Centre National de la Recherche Scientifique (CNRS), the University of Lille, and the ANR PADISC (ANR-20- CE19-0021) is received. Support by EuroNanoMed III (GSkin) is also acknowledged.

Declarations

Conflict of interest Sabine Szunerits is an editor of Analytical and Bioanalytical Chemistry but was not involved in the peer review of this paper. The other authors have no conflict of interest to declare.

References

1. Desai SB, Madhvapathy SR, Sachid AB, Llinas JP, Wang Q, Ahn GH, et al. MoS_2 transistors with 1-nanometer gate lengths. Science. 2016;354:99–102.
2. Ge X, Xia Z, Guo S. Recent advances on black phosphorus for biomedicine and biosensing. Adv Funct Mater. 2019;29:1900318.
3. Jing X, Illarionov Y, Yalon E, Zhou P, Grasser T, Shi Y, et al. Engineering field effect transistors with 2D semiconducting channels: status and prospects. Adv Funct Mater. 2020;30:1901971.
4. Meng Z, Stolz RM, Mendecki L, Miricica KA. Electrically-transduced chemical sensors based on two-dimensional nanomaterials. Chem Rev. 2019;119:478.
5. Béraud A, Sauvage M, Bazán CM, Tie M, Bencherif M, Bouilly D. Graphene field-effect transistors as bioanalytical sensors: design, operation and performance. Analyst. 2021;146:403.
6. Mohanty N, Berry V. Graphene-based single-bacterium resolution biodevice and DNA transistor: interfacing graphene derivatives with nanoscale and microscale biocomponents. Nano Lett. 2008;8:4469.
7. Palaniappan A, Goh WH, Tey JN, Wijaya IPM, Moochhala SM, Liedberg B, et al. Aligned carbon nanotubes on quartz substrate for liquid gated biosensing. Biosens Bioelectron. 2010;25:1989–93.

8. Palaniappan A, Goh WH, Fam DWH, Rajaseger G, Chan CEZ, Hanson BJ, et al. Label-free electronic detection of bio-toxins using aligned carbon nanotubes. Biosens Bioelectron. 2013;43:143–7.
9. Lerner MB, Matsunaga F, Han GH, Hong SJ, Xi J, Crook A, et al. Scalable production of highly sensitive nanosensors based on graphene functionalized with a designed G protein-coupled receptor. Nano Lett. 2014;14:27091.
10. Kwong Hong Tsang D, Lieberthal TJ, Watts C, Dunlop IE, Ramadan S, del Rio Hernandez AE, et al. Chemically functionalised graphene FET biosensor for the label-free sensing of exosomes. Sci Rep. 2019;9:1–10.
11. Hao Z, Pan Y, Shao W, Lin Q, Zhao X. Graphene-based fully integrated portable nanosensing system for on-line detection of cytokine biomarkers in saliva. Biosens Bioelectron. 2019;134:16.
12. Wei W, Pallecchi E, Haque S, Borini S, Avramovic V, Centeno A, et al. Mechanically robust 39 GHz cut-off frequency graphene field effect transistors on flexible substrates. Nanoscale. 2016;8(8):14097–103.
13. Wang B, Zhao C, Wan Z, Yang K-A, Cheng X, Liu W, et al. Wearable aptamer-field-effect transistor sensing system for noninvasive cortisol monitoring. Sci Adv. 2022;8:eabk0967.
14. Zhao C, Man T, Cao Y, Weiss PS, Monbouquette HG, Andrews AM. Flexible and implantable polyimide aptamer-field-effect transistor biosensors. ACS Sens. 2022;7:3644–53.
15. Park SJ, Kwon OS, Lee SH, Song HS, Park TH, Jang J. Ultrasensitive flexible graphene based field-effect transistor (FET)-type bioelectronic nose. Nano Lett. 2012;12:5082–90.
16. Jewel M, Siddiquee T, Islam M. Flexible graphene field effect transistor with graphene oxide dielectric on polyimide substrate. Int Conf Electr Inf Commun Technol (EICT). 2014. https://doi.org/10.1109/EICT.2014.677783418994804.
17. Bai J, Liao L, Zhou H, Cheng R, Liu L, Huang Y, et al. Top-gated chemical vapor deposition grown graphene transistors with current saturation. Nano Lett. 2011;11:2555–9.
18. Guerriero E, Pedrinazzi P, Mansouri A, Habibpour O, Winters M, Rorsman N, et al. High-gain graphene transistors with a thin AlOx top-gate oxide. Sci Rep. 2017;2419:1–7.
19. Yogeswaran N, Hosseini ES, Dahiya R. Graphene based low voltage field effect transistor coupled with biodegradable piezoelectric material based dynamic pressure sensor. ACS Appl Mater Interfaces. 2020;12:54035.
20. Wang Z, Hao Z, Yu S, Huang C, Pan Y, Zhao X. A wearable and deformable graphene-based affinity nanosensor for monitoring of cytokines in biofluids. Nanomaterials. 2020;10:1503.
21. Zhang X, Pu Z, Su X, Li C, Zheng H, Li D. Flexible organic field-effect transistors-based biosensors: progress and perspectives. Anal Bioanal Chem. 2023;415:1607–25.
22. Mishyn V, Rodrigues T, Leroux YR, Aspermair P, Happy H, Bintinger J, et al. Controlled covalent functionalization of a graphene-channel of a field effect transistor as an ideal platform for (bio)sensing applications. Nanoscale Horiz. 2021;6:819–29.
23. Rodrigues T, Mishyn V, Leroux YR, Butruille L, Woitrain E, Barras A, et al. Highly performing graphene-based field effect transistor for the differentiation between mild-moderate-severe myocardial injury. Nano Today. 2022;43:101391.
24. Mishyn V, Hugo A, Rodrigues T, Aspermair P, Happy H, Marques L, et al. The holy grail of pyrene-based surface ligands on the sensitivity of graphene-based field effect transistors. Sens Diagn. 2021;1:235–44.
25. Hugo A, Rodrigues T, Mader JK, Knoll W, Bouchiat V, Boukherroub R, et al. Matrix metalloproteinase sensing in wound fluids: are graphene-based field effect transistors a viable alternative? Biosensors and Bioelectronics: X. 2023;13:100305.
26. Rodrigues T, Curti F, Leroux YR, Barras A, Pagneux Q, Happy H, et al. Discovery of a peptide nucleic acid (PNA) aptamer for cardiac troponin I: substituting DNA with neutral PNA maintains picomolar affinity and improves performances for electronic sensing with graphene field-effect transistors (gFET). Nano Today. 2023;50:101840.
27. Hugo A, Rodrigues T, Mader JK, Knoll W, Bouchiat V, Boukherroub R, et al. Matrix metalloproteinase sensing in wound fluids: are graphene-based field effect transistors a viable alternative. Biosens Bioelectron X. 2023;13:100305.
28. Gao J, Gao Y, Han Y, Pang J, Wang C, Wang Y, et al. Ultrasensitive label-free MiRNA sensing based on a flexible graphene field-effect transistor without functionalization. ACS Appl Electron Mater. 2020;2:1090–8.
29. Kesler V, Murmann B, Soh HT. Going beyond the Debye length: overcoming charge screening limitations in next- generation bioelectronic sensors. ACS Nano. 2020;14:16194–201.
30. Gao N, Zhou W, Jiang X, Hong G, Fu T-M, Lieber CM. General strategy for biodetection in high ionic strength solutions using transistor-based nanoelectronic sensors. Nano Lett. 2015;15:2143–8.
31. Goldsmith BR, Locascio L, Gao Y, Lerner M, Walker A, Lerner J, et al. Digital biosensing by foundry-fabricated graphene sensors. Sci Rep. 2019;9:434.
32. Gokturk PA, Sujanani R, Qian J, Wang Y, Katz LE, Freema BD, et al. The Donnan potential revealed. Nat Commun. 2022;13:5880.
33. Song J, Dailey J, Li H, Jang H-J, Zhang P, Tza-Huei Wang J, et al. Extended solution gate OFET-based biosensor for label-free glial fibrillary acidic protein detection with polyethylene glycol-containing bioreceptor layer. Adv Funct Mater. 2017;27:1606506.
34. Montaigne D, Marechal X, Modine T, Coisne A, Mouton S, Fayad G, et al. Daytime variation of perioperative myocardial injury in cardiac surgery and its prevention by Rev-Erbα antagonism: a single-centre propensity-matched cohort study and a randomised study. Lancet. 2018;391(10115):59–69.
35. Jiang C, Wang HR, Liu N, Luo X, Davis JJ. Antifouling strategies for selective in vitro and in vivo sensing. Chem Rev. 2020;120:3852–89.
36. Russo MJ, Han M, Desroches PE, Manasa CS, Dennaoui J, Quigley AF, et al. Antifouling strategies for electrochemical biosensing: mechanisms and performance toward point of care based diagnostic applications. ACS Sens. 2021;6:1482–507.
37. Hwang MT, Heiranian M, Kim Y, You S, Leem J, Taqieddin A, et al. Ultrasensitive detection of nucleic acids using deformed graphene channel field effect biosensors. Nat Commun. 2020;11:1543.
38. Vu C-A, Chen W-Y, et al. Predicting future prospects of aptamers in field-effect transistor biosensors. Molecules. 2020;25:680.
39. Hasegawa H, Savory N, Abe K, Ikebukuro K. Methods for improving aptamer binding affinity. Molecules. 2016;2:421.
40. Hao Z, Pan Y, Huang C, Wang Z, Lin Q, Zhao X, et al. Modulating the linker immobilization density on aptameric graphene field effect transistors using an electric field. ACS Sens. 2020;5:2503–13.
41. Ohno Y, Maehashi K, Matsumoto K. Label-free biosensors based on aptamer-modified graphene field-effect transistors. J Am Chem Soc. 2010;132:18012.
42. Kim DJ, Park H-C, Soh IY, Jung J-H, Yoon OJ, Park J-S, et al. Electrical graphene aptasensor for ultra-sensitive detection of anthrax toxin with amplified signal transduction. Small. 2013;9:3352–60.
43. Mazarin de Moraes AC, Kubota LT. Recent trends in field-effect transistors-based immunosensors. Chemosensors. 2016;4:20.
44. Pagneux Q, Roussel A, Saada H, Cambillau C, Amigues B, Delauzun V, et al. SARS-CoV-2 detection using a nanobodyfunctionalized voltammetric device. Commun Med. 2022;2:56.
45. Guo K, Wustoni S, Kokul A, Diaz Galicia E, Moser M, Hama A, et al. Rapid single-molecule detection of COVID-19 and MERS

antigens via nanobody-functionalized organic electrochemical transistors. Nat Biomed Eng. 2021;5:666–77.
46. Gonzalez-Sapienza G, Rossotti MA, Tabares-da Rosa S. Single-domain antibodies as versatile affinity reagents for analytical and diagnostic applications. Front Immunol. 2017;8:977.
47. Muyldermans S. Applications of nanobodies. Annu Rev Anim Biosci. 2021;9:401–21.
48. Cheng S, Hotani K, Hideshima S, Kuroiwa S, Nakanishi T, Hashimoto M, et al. Field effect transistor biosensor using antigen binding fragment for detecting tumor marker in human serum. Materials. 2014;7:2490–500.
49. Suderman R, Rice DA, Gibson SD, Strick EJ, Chao D. Development of polyol-responsive antibody mimetics for single-step protein purification. Protein Expr Purif. 2017;134:114–24.
50. Pagneux Q, Garnier N, Fabregue M, Sharkaoui S, Mazzoli S, Engelmann I, et al. nanoCLAMP potently neutralizes SARS-CoV-2 and protects K18-hACE2 mice from infection. bioRxiv. 2023. https://doi.org/10.1101/2023.04.03.535401.